European Rotorcraft Forum

A STUDY TO EXAMINE EFFECTS OF THE INFLOW INTERFERENCE ON INDUCED POWER USING COMBINED MOMENTUM AND SIMPLE VORTEX THEORY INFLOW MODEL

Feyyaz Guner†
feyyazguner@gatech.edu
PhD Graduate

Jahnvi Hariani
jhariani3@gatech.edu
Undergraduate Researcher

J. V. R. Prasad
jvr.prasad@aerospace.gatech.edu
Professor

Georgia Institute of Technology
Atlanta, GA, US

Abstract
This paper uses a recently developed combined momentum theory and simple vortex theory (CMTSVT) inflow model to study effects of rotor-on-rotor inflow interference on induced power predictions for different multi-rotor configurations with varying overlapping areas. The validation with the Harrington coaxial rotor shows that this analytical model, although simple, can capture the overall rotor-on-rotor wake interference effects in the estimation of rotor power, without a need for its coupling with a blade element rotor model. The first harmonic self-induced and interference inflow components of individual rotors are also available for further exploration of the different multi-rotor configurations. Hence, the CMTSVT model can serve as a viable tool for rapid estimation of rotor-on-rotor interference on overall power required in the early design stages of vehicle configuration and sizing trade studies.

1. NOMENCLATURE

C_T	aerodynamic thrust coefficient
C_M, C_L	aerodynamic pitch moment coefficient and roll moment coefficient, respectively
$\bar{r}$	nondimensional radial blade coordinate
μ	advance ratio
λ_f	free-stream component of inflow
χ	the wake skew angle
ψ	azimuth angle
$\bar{\Gamma}$	nondimensional circulation
σ	rotor solidity
f	flat-plate parasite-drag area
R	rotor radius
Ω	angular velocity (rad/s)

2. INTRODUCTION

Due to substantial interest towards advanced air mobility (AAM) or urban air mobility (UAM), many new vehicle concepts are emerging in the market. These vehicles undergo numerous trial and error process from conceptual design phase to the first flying prototype. The design supported by the high-fidelity simulations and wind tunnel tests requires a certain design maturity that may lead to an early decision to finalize the vehicle configuration. Analytical tools, which are still used in the development of conventional configurations, should be adopted for these new vehicles consisting of more than one lifting rotor to support several design phases.

New vehicle concepts for UAM or AAM inherently consist of multi-rotor configurations and operate within a complex flow field. These new vehicles have rotor-on-rotor and other aerodynamic interference effects. These complex effects might be severe depending on the configuration. Thus, they should be introduced as early as possible to design phase for guiding the design engineers in determining the best possible vehicle configuration.

† Currently a postdoctoral researcher at German Aerospace Center (DLR). Email: feyyaz.guener@dlr.de

Higher-order wake models such as CFD, free-vortex wake, VVPM, and hybrid modelling approaches are often used to capture complex aerodynamic interference effects[1–13]. Alternatively, one can use analytical finite state multi-rotor inflow models based on superposition approaches that capture fundamental interference effects among the rotors[14–16]. More recently, a new multi-rotor inflow model known as combined momentum theory and simple vortex theory (CMTSVT) has been developed[17]. The CMTSVT takes advantage of simplicity of the momentum theory and combines it with a simple vortex theory to account for rotor-on-rotor inflow interference. In addition to rotor-on-rotor inflow interference, CMTSVT can predict interference inflow for any surface near the rotor. Because of its numerical efficiency, modular structure, and simplicity, CMTSVT is an ideal candidate to be used in the early design phases of these advanced configurations.

In this study, combined momentum and simple vortex theory inflow model is used to study the effect of inflow interference on the induced power. First, the model is validated against experimental data of a coaxial rotor in hover and forward flight. Then, different dual-rotor and quad-rotor configurations with and without partial overlap are examined. In addition to total induced power predictions, induced power due to self-induced inflow and interference inflow are provided, along with first harmonic inflow components, to gain further insight.

3. COMBINED MOMENTUM THEORY AND SIMPLE VORTEX THEORY INFLOW MODEL

The detailed description of the combined momentum theory and simple vortex theory (CMTSVT) inflow model is provided by Guner and Prasad in Ref. 17. The model takes advantage of simplicity of the momentum theory and a rigid wake vortex theory to arrive at a model that includes some of the fundamental rotor-on-rotor interference effects. The current version of the model can predict steady-state self-induced inflow and interference inflow components of generic multi-rotor configurations.

The CMTSVT follows the output-coupled model structure. The total inflow on a rotor is described as a summation of self-induced inflow and interference inflow due to other rotors, i.e., $\lambda(\bar{r},\psi) = \lambda^S(\bar{r},\psi) + \lambda^I(\bar{r},\psi)$. After approximating the inflow distribution with the first harmonic inflow expansion, the inflow distribution of *j*th rotor is expressed as:

$$\lambda^j(\bar{r},\psi) = \left(\lambda_0^{j,S} + \lambda_0^{j,I}\right) + \left(\lambda_{1c}^{j,S} + \lambda_{1c}^{j,I}\right)\bar{r}\cos\psi + \left(\lambda_{1s}^{j,S} + \lambda_{1s}^{j,I}\right)\bar{r}\sin\psi \quad (1)$$

In Eq. (1), superscripts S and I refer to self-induced and interference inflow components, respectively, whereas superscript j is the rotor indexing. The total flow passing through each rotor must be modified to satisfy continuity as interference inflow components provide additional air mass to each rotor. By considering this, the interference inflow is allowed to affect magnitude of the self-induced inflow and its effect solely depends on the magnitude of the interference inflow. The self-induced uniform inflow of *j*th rotor is calculated by Eq. (2).

$$\lambda_0^{j,S} = C_T^j / \left(2V_T^j\right) \quad (2)$$

where

$$V_T^j = \sqrt{(\mu^j)^2 + \left(\lambda_f^j + \lambda_0^j\right)^2}$$

$$\lambda_0^j = \lambda_0^{j,S} + \lambda_0^{j,I}$$

An iterative process is needed to solve for the self-induced uniform inflow component of each rotor (λ_0^S) until all self-induced and interference uniform inflow components converge. After this convergence, the first harmonic inflow components of *j*th rotor are obtained from the modified dynamic inflow formula of Pitt and Peters as follows[18]:

$$\lambda_{1c}^j = \lambda_{1c}^{j,S} + \lambda_{1c}^{j,I} \quad (3)$$

$$\lambda_{1s}^j = \lambda_{1s}^{j,S} + \lambda_{1s}^{j,I} \quad (4)$$

where

$$\lambda_{1c}^{j,S} = \frac{15\pi}{64V_T^j}\tan\frac{\chi^j}{2}C_T^j - \frac{4\cos\chi^j}{V^j(1+\cos\chi^j)}C_M^j$$

$$\lambda_{1s}^{j,S} = -\frac{4}{V^j(1+\cos\chi^j)}C_L^j$$

$$V^j = \frac{(\mu^j)^2 + \left(\lambda_f^j + \lambda_0^j\right)\left(\lambda_f^j + 2\lambda_0^j\right)}{V_T^j}$$

$$\chi^j = \tan^{-1}\frac{\mu^j}{\lambda_f^j + \lambda_0^j}$$

The first harmonic inflow components $\left(\lambda_0^{j,I}, \lambda_{1c}^{j,I}, \lambda_{1s}^{j,I}\right)$ of *j*th rotor are extracted from the interference inflow distribution that is calculated using a simple vortex theory formulated by Heyson[19]. He showed that induced velocities near a lifting rotor become available using the Biot-Savart law as a single integral, which only depends on the prescribed rigid wake geometry. Using Heyson's formula[19], interference inflow is calculated as:

$$\lambda^I = -\frac{1}{4\pi}\int_0^{2\pi} F(\psi)\frac{1-(x\cos\psi + y\sin\psi) + R_c\sin\chi\cos\psi}{[R_c + (\cos\psi - x)\sin\chi + z\cos\chi]R_c}d\psi \quad (5)$$

where

$$F(\psi) = \gamma_0 + \gamma_{1c}\cos\psi + \gamma_{1s}\sin\psi$$

$$R_c = \sqrt{1 + x^2 + y^2 + z^2 - 2(x\cos\psi + y\sin\psi)}$$

In Eq. (5), x, y, z represent Cartesian coordinates normalized by rotor radius. The vorticity variation around the azimuth is described as $F(\psi)$. Here, uniform (γ_0), cosine (γ_{1c}) and sine (γ_{1s}) parts of the vorticity are associated to C_T, C_M, and C_L using the following equations[18].

(6) $$\gamma_0 = \frac{C_T}{V_T(1-1.5\mu^2)} + \frac{3\mu C_L}{V_T(1-1.5\mu^2)}$$

(7) $$\gamma_{1c} = -\frac{3C_M}{V_T}$$

(8) $$\gamma_{1s} = -\frac{3C_L}{V_T(1-1.5\mu^2)} - \frac{1.5\mu C_T}{V_T(1-1.5\mu^2)}$$

After finding interference inflow distribution at a rotor, interference uniform, longitudinal, and lateral inflow components are approximated using Eqs. (9), (10), and (11) as

(9) $$\lambda_0^I = \frac{1}{\pi}\int_0^{2\pi}\int_0^1 \lambda^I(\bar{r},\psi)\,\bar{r}\,d\bar{r}\,d\psi$$

(10) $$\lambda_{1c}^I = \frac{4}{\pi}\int_0^{2\pi}\int_0^1 \lambda^I(\bar{r},\psi)\,\bar{r}^2\cos\psi\,d\bar{r}\,d\psi$$

(11) $$\lambda_{1s}^I = \frac{4}{\pi}\int_0^{2\pi}\int_0^1 \lambda^I(\bar{r},\psi)\,\bar{r}^2\sin\psi\,d\bar{r}\,d\psi$$

To obtain the total interference inflow corresponding to every rotor, calculations must be repeated for $(N-1)\times N$ times for a multi-rotor configuration with N number of rotors. In Eq. (12), indexing is provided for *j*th rotor.

(12) $$\{\lambda_0^{j,I}, \lambda_{1c}^{j,I}, \lambda_{1s}^{j,I}\} = \sum_{k=1,\ k\neq j}^{N}\{\lambda_0^{k,I}, \lambda_{1c}^{k,I}, \lambda_{1s}^{k,I}\}$$

The developed combined momentum theory and simple vortex theory (CMTSVT) inflow model has been previously validated[17] against the Velocity Potential Superposition Inflow Model (VPSIM), which was shown to correlate well with the higher order wake models such as Viscous Vortex Particle Method (VVPM) and GT-Hybrid[15, 16, 20, 21].

4. SIMULATION PROCEDURE

For evaluation of the CMTSVT inflow model, two vehicle configuration cases, viz., the dual rotor configuration and the quad-rotor configuration, are considered. The dual rotor configuration uses the geometry of the Harrington coaxial rotor[22] to compare and validate the obtained results against the experimental results. The vertical separation distance between the rotors is set to 0.19 radius ($0.19R$), and results are obtained for both hover, and forward flight, for the coaxial configuration. The longitudinal separation distance is then varied from 0 (coaxial) to $2R$ (tandem configuration with no overlap) to examine the effects of rotor overlap on induced velocity and induced power. For all dual rotor configurations, a torque balance between the two rotors is achieved by trimming and varying the thrust sharing ratio. For example, in the case of coaxial rotor, this ratio settles around 1:0.75 for the range of thrust coefficients considered in hover with the upper rotor producing more thrust. As the advance ratio is increased, the ratio gets closer to 1:1 with both rotors producing equal amounts of thrust. The coefficient of power (C_P), equal for both rotors due to torque balancing, is calculated for each rotor using the following equation:

(13) $$C_P = kC_{P,ind} + \frac{\sigma C_{D0}}{8}(1 + 4.65\mu^2) + 0.5\mu^3\left(\frac{f}{A}\right)$$

where

$$C_{P,ind} = \frac{1}{2\pi}\int_0^{2\pi}\int_0^1 (\bar{r} + \mu sin\psi)\bar{\Gamma}\lambda(\bar{r},\psi)\,d\bar{r}\,d\psi$$

$$C_{D0} = 0.0115 + 0.3\left(\frac{6C_T}{a\sigma}\right)^2$$

and '*k*' is a correction factor selected as 1.15 in this study to account for flow swirl and non-uniform inflow due to blade twist in hover. Additionally, *'A'* is the rotor disk area and λ is the total nondimensional inflow distribution obtained from the model at a particular radial and azimuthal location. The azimuthal variation of the nondimensional circulation is given by Eq. (14) as

(14) $$\bar{\Gamma}(\psi) = \bar{\Gamma_0} + \bar{\Gamma}_{1c}cos\psi + \bar{\Gamma}_{1s}sin\psi$$

Here, $\bar{\Gamma_0}$ is the mean rotor bound circulation, and $\bar{\Gamma}_{1c}$ and $\bar{\Gamma}_{1s}$ respectively, are the longitudinal and lateral variations of the same. These circulations are found by taking the products of corresponding vorticity strengths (γ) with the mass flow parameter (V_T^j) associated with the rotor mean inflow[18].

The lift curve slope (a) is taken to be equal to 5.73, with rotor solidity (σ) equalling 0.027 for the Harrington rotor[23]. The coefficient 0.0115 is calculated by matching the computed C_P value at zero thrust to the experimental value of 0.000777. For forward flight, a flat-plate parasite-drag area of 10 square feet is used along with a tip speed of 469 ft/s and a constant weight coefficient C_W of 0.0048[24] (C_T=C_W in hover but has a drag component in forward flight). The results are converted to horsepower for validation against experimental data.

A tandem rotor configuration[24] with a rotor disc diameter of 15 ft (Figure 1) is also used to validate the model against experimental data in hover. In this configuration, there is no vertical separation as well as overlap between the two rotors. As there is no rotor wake interference between the rotors, each

rotor produces the same amount of thrust and has a solidity of 0.054[24]. C_P is calculated using Eq. (13), with $C_{D0} = 0.004 + 0.3\left(\frac{6C_T}{a\sigma}\right)^2$.

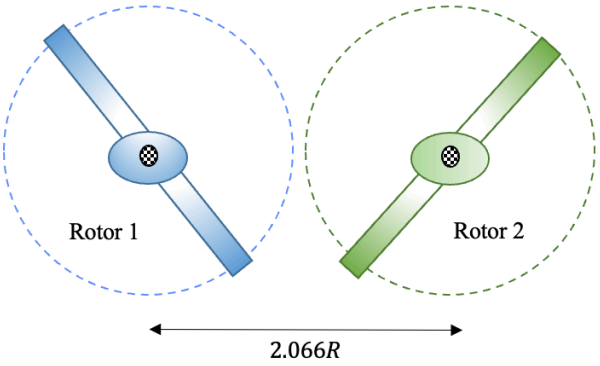

Figure 1. Tandem rotor configuration.[24]

For the quadrotor configuration, the two cases considered for this study are partial and no overlap, as shown in Figures 2 and 3, respectively.

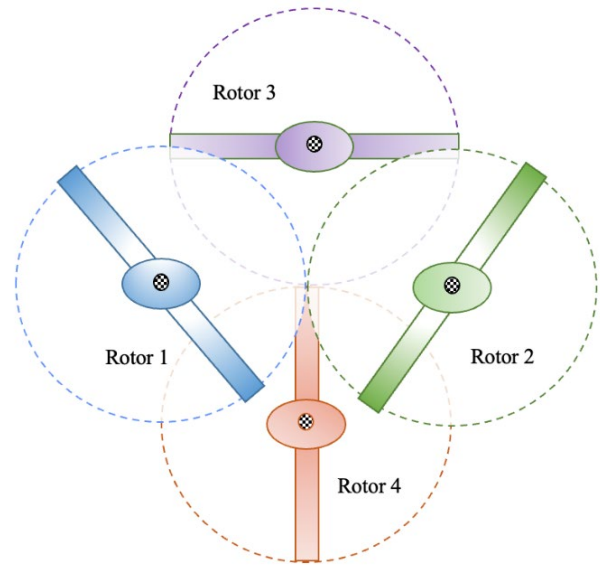

(a) Top View

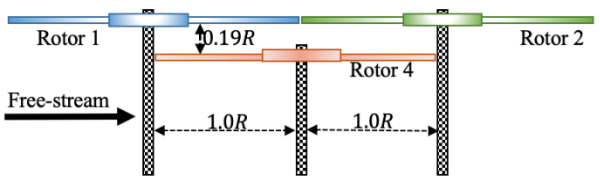

(b) Side View

Figure 2. Quad-rotor configuration with overlap.

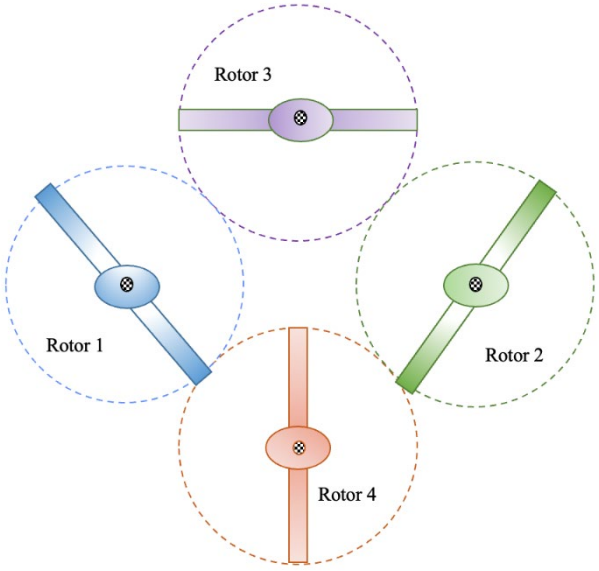

(a) Top View

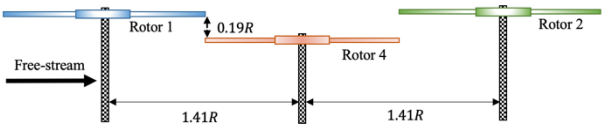

(b) Side View

Figure 3. Quad-rotor configuration without overlap.

In the quad-rotor case, trimming is performed such that the sum of torques of the two upper rotors is in balance with the sum of torques of the two lower rotors. While the thrust produced by rotor 3 is taken to be equal to the thrust produced by rotor 4 (lower rotors) in all cases due to flow symmetry, this is not true for the two upper rotors. Although rotors 1 and 2 produce equal amounts of thrust during hover, rotor 2 acts considerably under the influence of rotor 1 during forward flight, producing much lesser thrust. Thus, their thrust sharing ratio changes to approximately 1:0.68 for the no overlap configuration, and to 1:0.50 for the configuration with partial overlap during forward flight. These thrust sharing ratios of the quad-rotor configurations are used to calculate power and plot results for various advance ratios. The flat-plate parasite-drag area and tip speed used for this process are the same as that of the coaxial dual-rotor configuration.

5. RESULTS AND DISCUSSION

5.1. Coaxial Rotor Configuration

The purpose of this part of the study is to validate the obtained total power results against experimental data for both hover and forward flight. As shown in Figure 4, the total power predictions from CMTSVT are quite similar to the Harrington rotor experimental

results despite it being a model with a simple implementation. The average percentage error between the experimental and predicted power (C_P) results is about 3%. It is expected that the observed discrepancy between the CMTSVT model prediction and the experimental data can be further reduced with the inclusion of wake contraction and viscous decay effects, which are not considered in this study to retain the simplicity of the model.

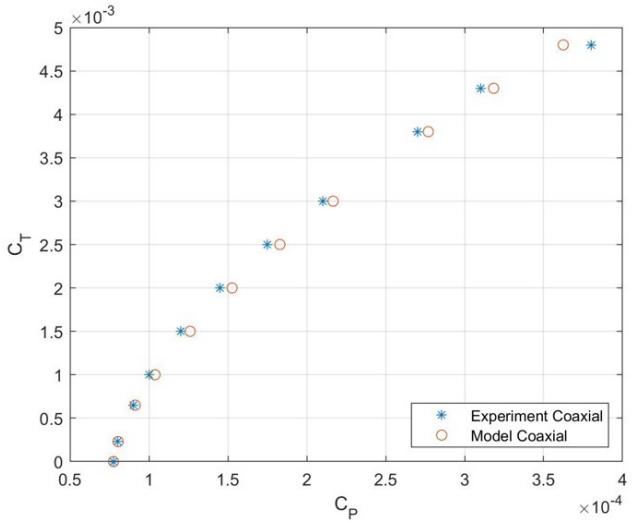

Figure 4. Coaxial rotor C_T vs. C_P for hover with a thrust sharing ratio around 1:0.75.

In the next part, advance ratio is varied from 0 to 0.24 for power predictions of the Harrington coaxial rotor, keeping the total weight coefficient at a constant value of 0.0048. As seen in Figure 5, the predictions correlate well with experimental data even for various advance ratios.

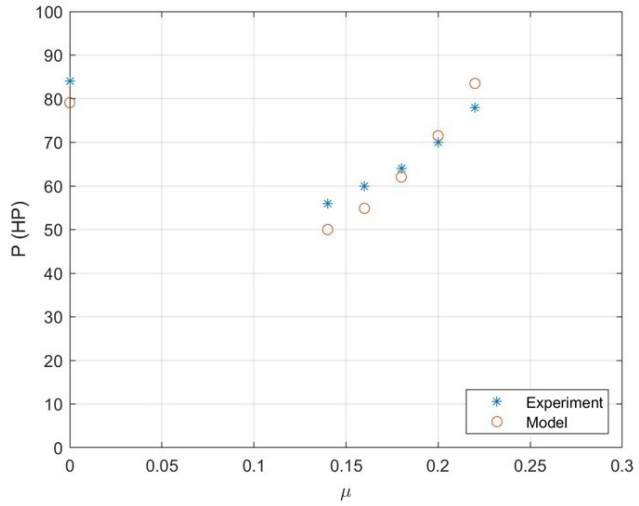

Figure 5. Power vs. advance ratio for coaxial rotor in forward flight with $C_W = 0.0048$.

5.2. Effect of Longitudinal Separation

In analyses of multi-rotor inflow models, Ref. 16 has shown that longitudinal inflow components exist even in hover if rotors are partially overlapping longitudinally. Since it affects the vehicle's stability, this phenomenon is crucial to capture[25]. The effect of only longitudinal separation is analysed in the study for the dual rotor configuration since the effect of lateral separation will be similar, introducing lateral inflow components.

To study this effect, the longitudinal separation distance between the Harrington rotors is gradually increased from 0.0 to 2.0 rotor radius. The total thrust (equal to weight in hover) coefficient is set to 0.0048, while aerodynamic hub moments are set to 0.0. Figure 6 shows uniform and longitudinal inflow predictions for the lower rotor at various longitudinal overlap percentages. Figure 7 shows the same results for the upper rotor.

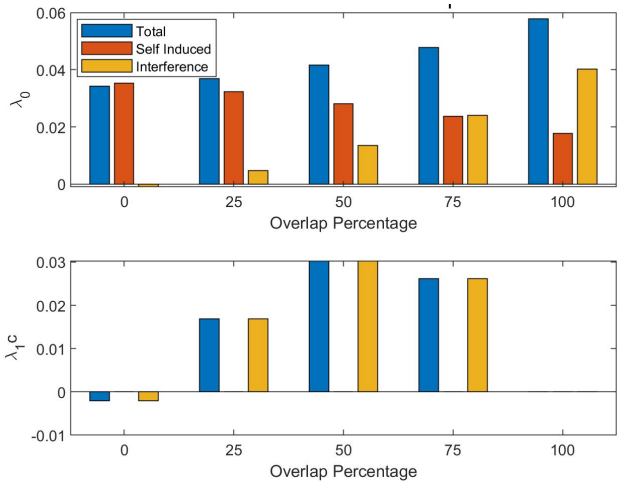

Figure 6. Uniform and longitudinal inflow predictions for the lower rotor at various longitudinal overlap percentages for $C_W = 0.0048$ in hover.

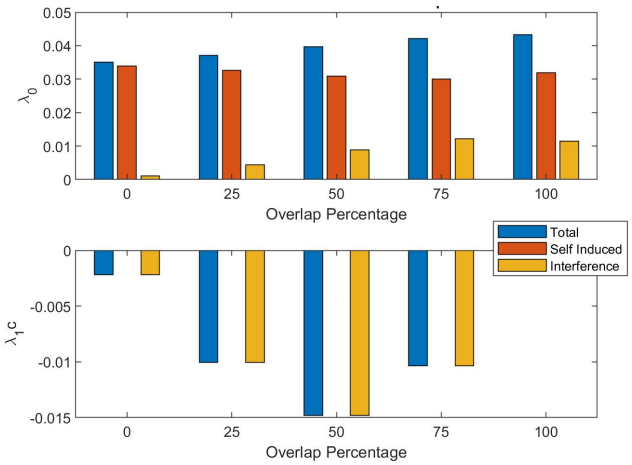

Figure 7. Uniform and longitudinal inflow predictions for the upper rotor at various longitudinal overlap percentages for $C_W = 0.0048$ in hover.

As seen in Figures 6 and 7, the model predicts only interference contribution for the longitudinal inflow components in both rotors. This implies that without the inflow interference, the model predicts zero longitudinal inflow components for the rotors regardless of the longitudinal separation distance, like a single rotor configuration without aerodynamic pitch moment. Since the longitudinal inflow components can become as large as the uniform inflow components in some cases (see Figure 6), they might significantly affect rotor performance and trim, hence, are important for consideration in design.

Figure 8 shows the predictions for total induced power for various longitudinal separation distances in hover. Interference contribution rises with increase in overlap percentage (or interference area) while longitudinal separation distance decreases. At 100% overlap (coaxial configuration), the contribution of interference inflow is almost equal to that of the self-induced inflow and cannot be neglected. In reality, this effect is expected to be smaller compared to the predictions using the CMTSVT model due to neglected real flow effects such as wake contraction and wake diffusion.

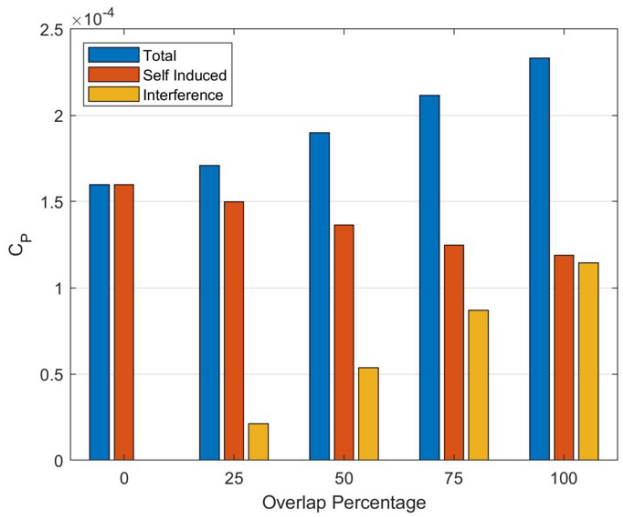

Figure 8. Total induced power predictions at $C_W = 0.0048$ in hover for various rotor overlap percentages.

Lastly, the total power predictions for a tandem rotor configuration[24], with the rotors not touching each other and without any vertical separation, are plotted against experimental data in Figure 9. Despite the model having a simple implementation (no coupling with a blade-element rotor model), the discrepancy between the predicted and experimental results[24] can be further reduced by coupling the CMTSVT with a blade-element rotor model.

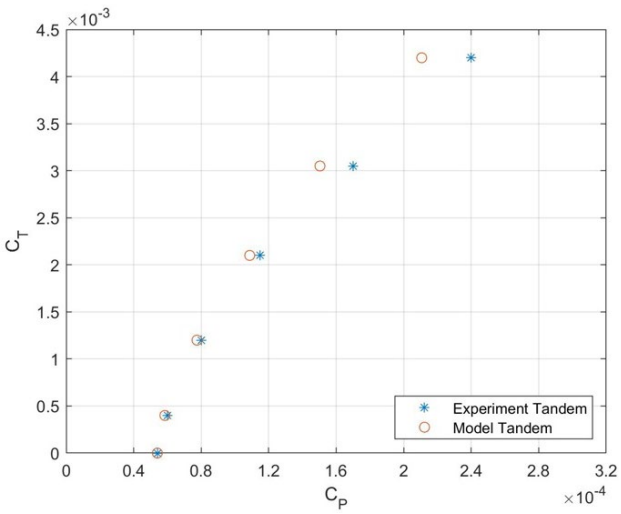

Figure 9. Tandem rotor[24] C_T vs. C_P for hover with a thrust sharing ratio of 1:1.

5.3. Quad-rotor Configurations

The CMTSVT is a generic inflow model that is applicable to any configuration. Two quad-rotor configurations with partial overlap and no overlap are used to demonstrate its capability. Inflow and power predictions of these quad-rotor configurations are also studied. Quad-rotor configurations with partial overlap and no overlap are shown in Figures 2 and 3, respectively. As discussed in section 4, there is a torque balance between the upper and lower rotors. Additionally, Figure 10 shows the predictions of total power (in HP) for the partial and no overlap cases at various advance ratios. The results obtained are higher for the partial overlap case as compared to no overlap, since the partial overlap case is subject to more interference effects.

Figure 11 shows the uniform, longitudinal, and lateral inflow components for all four rotors at zero and partial overlap for CW= 0.0048 in hover. Since rotors 1 and 2 are longitudinally separated, the lateral inflow components in Figure 11 (a) and (b) are of a very small order (10-19). For rotors 3 and 4 which are laterally separated, the same can be seen for longitudinal inflow components in Figure 11 (c) and (d). Similar to the dual rotor case, the model predicts zero longitudinal and lateral components if interference inflow is not taken into account.

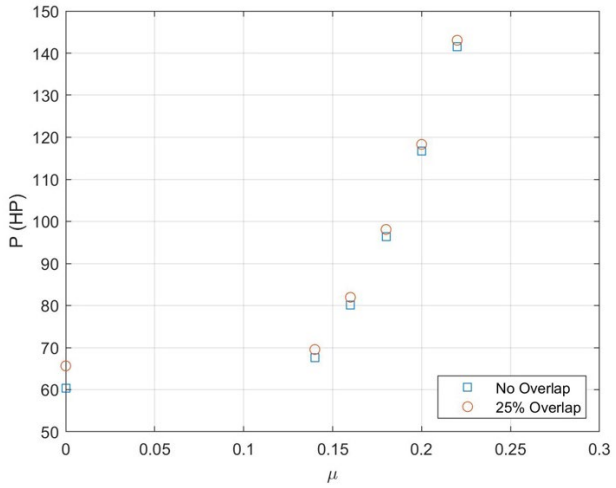

Figure 10. Power vs. advance ratio for quad-rotor configuration with zero and partial overlap at a constant $C_W = 0.0048$.

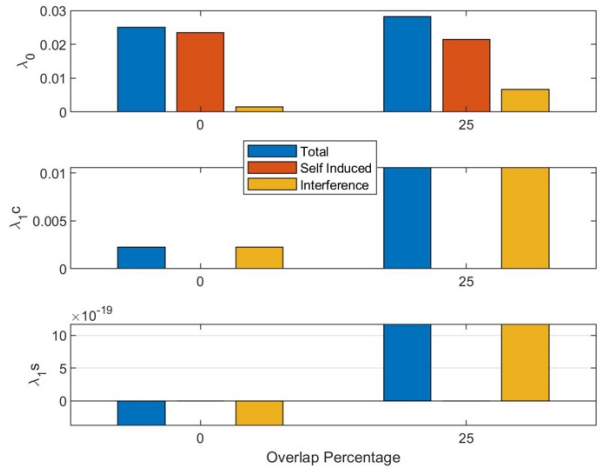

(a) Rotor 1

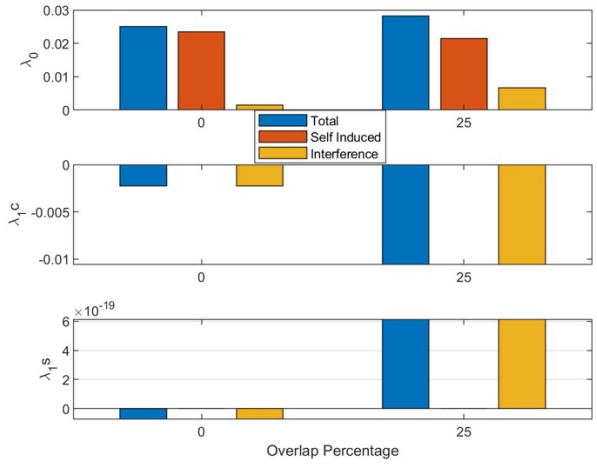

(b) Rotor 2

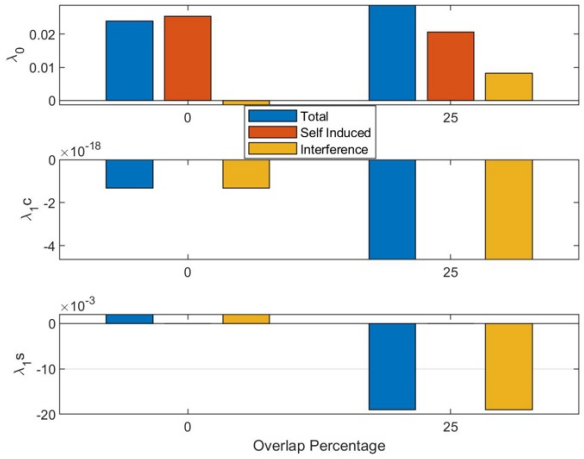

(c) Rotor 3

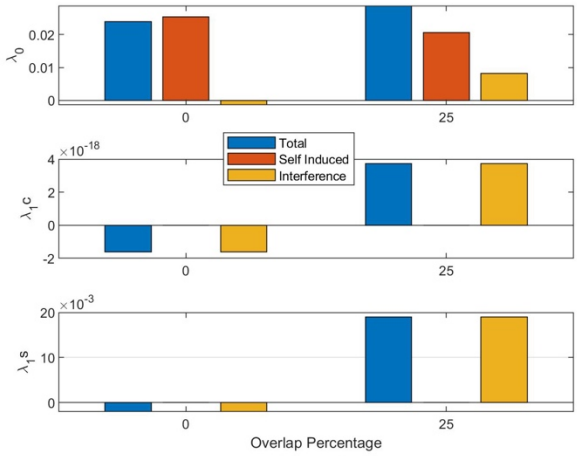

(d) Rotor 4

Figure 11. Uniform, longitudinal, and lateral inflow predictions for each rotor at zero and partial overlap for $C_W = 0.0048$ in hover.

Figure 12 shows the induced power predictions and interference inflow contributions for the upper and lower rotors in hover at a constant C_W of 0.0048. As overlap percentage and interference area increase, so does the contribution of interference inflow in the induced power. For the partial overlap case considered in this study, this contribution amounts to nearly 25% of the total power prediction.

The predictions below can be extended to forward flight to assess the contribution of interference in individual rotors at various advance ratios. As clear from the figures below, interference inflow plays a considerable role in induced power computations, and hence, is an important factor in the design cycle involving vehicle configuration and sizing trade studies.

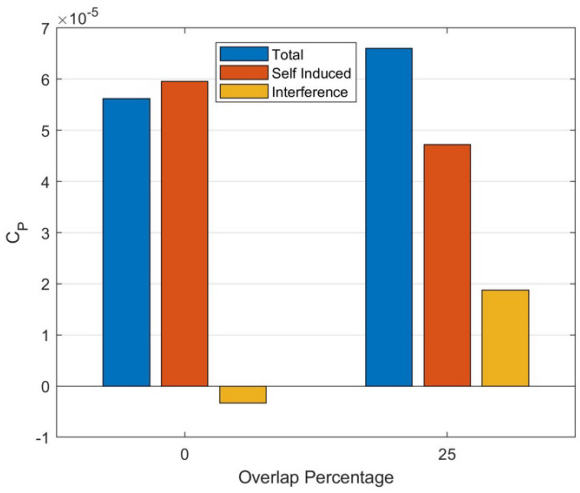

(a) Two lower rotors

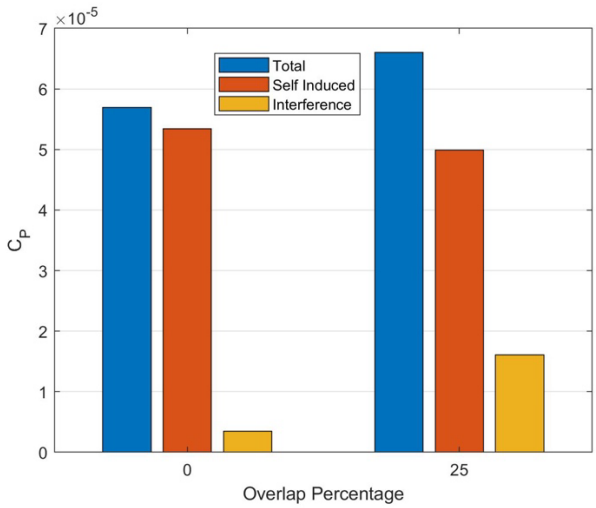

(b) Two upper rotors

Figure 12. Induced power predictions and interference contributions for lower and upper rotors in hover condition at $C_W = 0.0048$.

6. CONCLUDING REMARKS

A recently developed combined momentum theory and simple vortex theory (CMTSVT) inflow model for computing induced velocities at individual rotors of multi-rotor configurations is evaluated for its fidelity in the prediction of power required in trim at hover and various forward flight speeds. The CMTSVT benefits from its modular structure and simplified modeling approach, while capturing the fundamental interference effects.

The power predictions from the CMTSVT model are first correlated with wind tunnel test data available in the literature for a coaxial rotor in hover and several advance ratios. The model predictions of rotor power are found to be reasonably good, within acceptable errors in spite of the simplifying assumptions used in the CMTSVT inflow model development for its viability as a tool during the design cycles of advanced multi-rotor configurations. The variation of power required and induced velocity predictions of a dual rotor and a quadrotor with different rotor-to-rotor overlap ratios are found to be qualitatively correct. Further, the CMTSVT model is found to be computationally fast for its viability as a tool in the required rapid estimations of power in vehicle configuration and sizing trade studies. Further validation of the CMTSVT model induced velocity and power predictions with test data will enhance its viability for its routine use in design trade studies involving multi-rotor configurations.

7. ACKNOWLEDGMENTS

The financial support received by Jahnvi Hariani under a President's Undergraduate Research Award (PURA) at Georgia Tech during this study is gratefully acknowledged.

8. REFERENCES

[1] Kim, H. W. and Brown, R. E., "A Comparison of Coaxial and Conventional Rotor Performance," Journal of the American Helicopter Society, Vol. 55, (1), January 2010.

[2] Lakshminarayan, V. K. and Baeder, J. D., "High Resolution Computational Investigation of Trimmed Coaxial Rotor Aerodynamics in Hover," in Proceedings of the AHS International Specialists' Conference on Aeromechanics, San Francisco, CA, January 2008.

[3] He, C., and Zhao, J., "Modeling Rotor Wake Dynamics with Viscous Vortex Particle Method," AIAA Journal, Vol. 47, (4), April 2009, pp. 902–915.

[4] He, C., Syal, M., Tischler, M. B., and Juhasz, O., "State-space Inflow Model Identification from Viscous Vortex Particle Method for Advanced Rotorcraft Configurations," American Helicopter Society 73rd Annual Forum Proceedings, Fort Worth, Texas, May 2017.

[5] Bagai, A., and Leishman, J. G., "Free-Wake Analysis of Tandem, Tilt-Rotor and Coaxial Rotor Configurations," in Proceedings of the 51st Annual Forum, Fort Worth, Texas, May 1995.

[6] Bagai, A., Leishman, J. G., and Ananthan, S., "Free-Vortex Wake Predictions of the Vortex Ring State for Single-Rotor and Multi-Rotor Configurations," in Proceedings of the 58th Annual Forum, Montreal, Canada, June 2002.

[7] Wachspress, D. A., and Quackenbush, T. R., "Impact of Rotor Design on Coaxial Rotor

Performance, Wake Geometry and Noise," in Proceedings of the 62nd Annual Forum, Phoenix, AZ, May 2006.

[8] Rand, O., and Khromov, V., "Parametric Study of Dynamic Inflow for Single and Coaxial Rotor Systems," Journal of the American Helicopter Society, Vol. 63, (4), October 2018.

[9] Keller, J. D., McKillip, R. M., Wachspress, D. A., Tischler, M. B., and Juhasz, O., "A Free Wake Linear Inflow Model Extraction Procedure for Rotorcraft Analysis," American Helicopter Society 73rd Annual Forum Proceedings, Fort Worth, Texas, May 2017.

[10] Keller, J. D., McKillip, R. M., Wachspress, D. A., Tischler, M. B., and Juhasz, O., "Linearized Inflow and Interference Models from High Fidelity Free Wake Analysis for Modern Rotorcraft Configurations," Vertical Flight Society 75th Annual Forum Proceedings, Philadelphia, PA, May 2019.

[11] Egolf, T., Reed, E., Rajmohan, N., and Sankar, L., "A Hybrid CFD Method for Coaxial Rotor Performance Prediction in Forward Flight," in Proceedings of the AHS Aeromechanics Specialists' Conference, San Francisco, California, January 2010.

[12] Kim, J., Sankar, L. N., and Prasad, J. V. R., "Application of a Navier–Stokes Free Wake Hybrid Methodology to the Harrington Coaxial Rotor," Proceedings of the AHS Technical Meeting on Aeromechanics Design for Vertical Lift, San Francisco, CA, January 2016.

[13] Lee, J., Oh, S., Yee, K., and Kim, D. K., "Numerical Investigation on Overlap Effects of Tandem Rotors in Forward Flight," Int'l Journal of Aeronautical & Space Sciences, Vol. 10, (2), 2009.

[14] Kong, Y. B., Prasad, J. V. R., Sankar, L. N., and He, C., "Finite State Inflow Flow Model for Coaxial Rotor Configuration," Journal of the American Helicopter Society, Vol. 65, (3), July 2020.

[15] Guner, F., Kong, Y. B, Prasad, J. V. R., Peters, D. A., and He, C., "Development of Finite State Inflow Models for Multi-Rotor Configurations using Analytical Approach," in Proceedings of the AHS 74th Annual Forum, Phoenix, AZ, May 2018.

[16] Guner, F., Prasad, J. V. R., Sankar, L. N., Peters, D. A., and He, C., "Correlation of Finite State Multi-Rotor Dynamic Inflow Models with a High Fidelity Viscous Vortex Particle Method," Proceedings of the 44th European Rotorcraft Forum, Delft, Netherlands, September 2018.

[17] Guner, F., and Prasad, J. V. R., "Combined Momentum and Simple Vortex Theory Inflow Model for Multi-Rotor Configurations," Proceedings of the Vertical Flight Society's 9th Biennial Autonomous VTOL Technical Meeting, Virtual, January 2021.

[18] Zhao, J., Dynamic Wake Distortion Model for Helicopter Maneuvering Flight, Ph.D. thesis, Georgia Institute of Technology, March 2005.

[19] Heyson, H. H., "Equations for the Induced Velocities Near a Lifting Rotor with Nonuniform Azimuthwise Vorticity Distribution," NASA TN D-394, August 1960.

[20] Guner, F., Prasad, J. V. R., and He, C., "Finite State Multi-Rotor Wake Models Based on Superposition Approaches: PPSIM and VPSIM," in Proceedings of the 8th Asian/Australian Rotorcraft Forum, Ankara, Turkey, Oct. 30- Nov.2, 2019.

[21] Chen, P.-W., Guner, F., Sankar, L. N., Prasad, J. V. R., and He, C., "Calibration of Velocity Potential Superposition Inflow Model using Computational Fluid Dynamics Data," in Proceedings of the VFS Aeromechanics for Advanced Vertical Flight Technical Meeting, San Jose, CA, January 2020.

[22] Harrington, R., "Full Scale Tunnel Investigation of the Static Thrust Performance of a Coaxial Helicopter Rotor," NACA TN 2318, March 1951.

[23] M. Nowak, J. V. R. Prasad, H. Xin, and D. A. Peters, "A Potential Flow Model for Coaxial Rotors in Forward Flight," in Proceedings of the 39th European Rotorcraft Forum, Moscow, Russia, Sept. 2013.

[24] Dingeldein, R., Wind tunnel studies of the performance of multirotor configurations. TN 3236, NACA, August 1954.

[25] Amer, K. B., "Theory of Helicopter Damping in Pitch or Roll and Comparison with Flight Measurement," NACA, TN 2136, October 1948.